A Rotary Traveling Wave Ultrasonic Motor With Four Groups of Nested PZT Ceramics: Design and Performance Evaluation

Xuefeng Ma, Junkao Liu, Jie Deng, Qiang Liu, and Yingxiang Liu, *Senior Member, IEEE*

***Abstract*— This study proposes a rotary traveling wave ultrasonic motor utilizing the B (0, 5) axial bending mode of a ring-shaped stator. The proposed motor had a compact structure as only four groups of piezoelectric (PZT) ceramics were nested into the stator to produce a bending traveling wave, a new design method was proposed utilized less PZT ceramics to reduce the volume and to improve the mechanical output characteristics. The operating principle of the proposed motor was illustrated. The finite element analysis was performed to obtain the vibration modes and the motion trajectories of the stator. A prototype was manufactured to validate the operating principle. The two standing waves and the motion trajectories of the driving tips were measured. The results denoted that this motor obtained an output speed of 53.86 r/min under a preload of 0.69 N when the frequency and voltage were 24.86 kHz and 250 V_{p-p}, the maximum stall torque was tested as about 0.11 N · m under the preload of 3.14 N. Finally, this study was compared with a previous design and it was found that the volume was reduced markedly; furthermore, the no-load speed, the efficiency, the torque density and the power density were improved significantly.**

***Index Terms*— Axial bending mode, piezoelectric (PZT) ceramics nested structure, rotary ultrasonic motor (USM), traveling wave.**

I. Introduction

TRAVELING wave ultrasonic motor (USM) is an actuator based on high-frequency vibration of a stator that is pressed against a rotor [1]–[6]. It has been an important focus due to the merits of large power density, simple structure, self-locking when power-off and nonelectromagnetic radiation [7]–[11]. According to the structure of the traveling wave USM, it can be divided into the bonded-type and the sandwiched-type [12]. Among various bonded-type traveling wave USMs, the piezoelectric (PZT) ceramics are mostly glued with the stator through the adhesives, which have the advantage of simple structure [13], [14]. However, problems of adhesives failure and PZT ceramics fracture may easily happen because of the high-frequency vibration. Moreover, the d_{31} working mode of the PZT ceramics is widely utilized in various traveling wave USMs. It has a lower electromechanical coupling factor compared with the d_{33} working mode [15].

In order to overcome the shortcomings, it is innovative to excite the traveling wave by the sandwiched-type motor utilizing the d_{33} working mode of PZT ceramics. Theoretically speaking, the configuration of the sandwiched-type motor can achieve higher efficiency than the bonded-type traveling wave USM. However, the coupling interface exists between the sandwiched-type motor and the stator, which causes the deformation of the traveling wave, and the vibration energy is greatly consumed at the interface. Furthermore, the vibration modes of the motor and the stator need to be well matched to generate an ideal traveling wave, which leads to a difficult work of structure optimization [16].

In the previous work, a traveling wave USM composed of a ring-shaped stator nested with PZT ceramics was proposed to overcome the shortcomings of both the bonded-type motors and the sandwiched-type motors [17], in which the block springs were nested into the adjacent slots of the PZT ceramics to generate the preload forces. In this design, the d_{33} working mode was utilized to excite the axial vibration of the stator. The vibration mode matching was also simplified because of the utilization of the ring-shaped stator and the uniformly nested PZT ceramics. This prototype could generate a maximum torque of 7.96 N · m. However, 128 PZT ceramics and 64 spring blocks were nested into the stator to excite the traveling wave, which caused high weight and the large external diameter, and the manufacturing processes of the slots and the assembling processes of the PZT ceramics were also complicated.

In this new design, the first significant improvement is the reduction of PZT ceramics from 128 to 16, which not only reduces the difficulties of the manufacturing and assembling processes, but also reduces the weight and the volume. Four trapezoidal grooves are manufactured on a metal ring to nest the PZT ceramics, and the wedging blocks are used to generate the preload forces. With these significant improvements, the proposed traveling wave USM can be utilized as the driving component of the single-DOF robot joint.

Manuscript received November 19, 2019; accepted February 4, 2020. Date of publication February 7, 2020; date of current version June 29, 2020. This work was supported in part by the National Natural Science Foundation of China under Grant 51975162 and Grant 51622502 and in part by the Foundation for Innovative Research Groups of the National Natural Science Foundation of China under Grant 51521003. *(Corresponding author: Yingxiang Liu.)*

Xuefeng Ma, Junkao Liu, Jie Deng, and Yingxiang Liu are with the State Key Laboratory of Robotics and System, Harbin Institute of Technology, Harbin 150001, China (e-mail: liuyingxiang868@hit.edu.cn).

Qiang Liu is with the Changchun Institute of Optics, Fine Mechanics and Physics, Chinese Academy of Sciences, Changchun 130033, China.

Digital Object Identifier 10.1109/TUFFC.2020.2972307

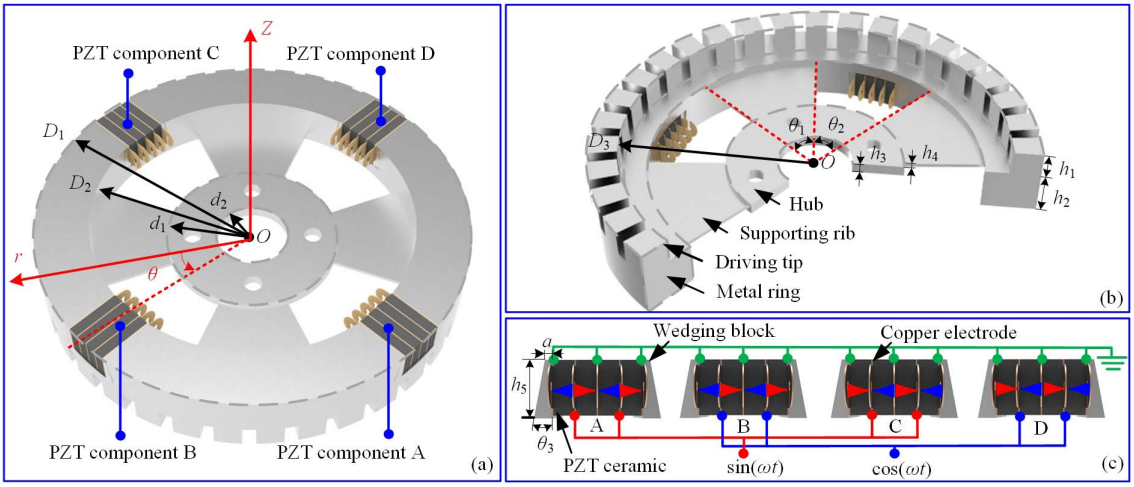

Fig. 1. Structure of the proposed traveling wave USM. (a) Ring-shape stator. (b) Cross-sectional view of the ring-shaped stator. (c) PZT polarizations and exciting methods.

This work is organized as follows. First, the operating principle of the proposed traveling wave USM is presented. Second, the structure and the manufacturing details are illustrated. Third, the mechanical characteristics of the prototype, including vibration modes, resonant frequencies and motion trajectories, are obtained through the finite element method (FEM). Finally, the mechanical characteristics of the prototype are tested and the merits of this prototype are discussed.

II. Structure of the Stator

The configuration of the proposed traveling wave USM is shown in Fig. 1. It consists of a ring-shape stator, four PZT components and four pairs of wedging blocks. The ring-shaped stator is composed of a metal ring, driving tips, supporting ribs and a hub. The ring and wedging blocks are made of aluminum alloy to effectively reduce the weight. The ring is connected to the hub through the supporting rib. The thickness of the supporting rib is designed to be much smaller than the ring and the hub, which intends to reduce the vibration transmitted to the base. The driving tips are perpendicular to the annular surface of the ring, which are used to amplify the vibration amplitudes.

One PZT component is made up of five copper electrodes with a thickness of 0.1 mm and four pieces of PZT ceramics with a thickness of 1.5 mm. The PZT ceramics are sandwiched among the adjacent copper electrodes. PZT components are bonded as following steps. First, the copper electrodes and the PZT ceramics are cleaned by acetone. Second, the components are placed as the order in Fig. 1(c). Third, the components are glued with each other through the epoxy adhesives. Finally, the PZT components are clamped by parallel-jaw vices for 24 h to solidify the epoxy adhesives. Polarization directions of the PZT ceramics are along with their thickness directions. The exciting voltages are applied to the PZT ceramics through the copper electrodes, and the d_{33} working modes of the PZT ceramics are adopted. The PZT components are nested to the trapezoidal grooves manufactured on the metal ring. Total thicknesses of the PZT components are manufactured to be 0.08-mm larger than the width of their nested trapezoidal grooves, and these thickness differences are used to generate the preload forces. The actual thickness differences can be compensated according to the ideal value by adding copper foil with a thickness of 0.01 mm or reducing the thickness of the copper electrode.

III. Operation Principle

The stator of the proposed traveling wave USM is ring-shape with an axial symmetry structure. The out-of-plane bending mode of the ring-shaped stator can be represented by B_{mn}, where m stands for the number of nodal diameters and n stands for the number of nodal circles.

The two orthogonal vibration mode functions of the out-of-plane bending mode can be described as

$$\phi_A(r,\theta) = J_n(r)\sin n\theta \tag{1}$$

$$\phi_B(r,\theta) = J_n(r)\cos n\theta \tag{2}$$

where r is the polar diameter of the particle in the cylindrical coordinate system, θ is the angular position and $J_n(r)$ is the nth-order Bessel function.

When two voltages are applied to the two groups of the PZT ceramics, respectively, the displacements can be described as follows:

$$\varpi_A(r,\theta,t) = \phi_A(r,\theta)q_A(t) = \zeta_A J_n(r)\sin n\theta\cos\omega_n t \tag{3}$$

$$\varpi_B(r,\theta,t) = \phi_B(r,\theta)q_B(t) = \zeta_B J_n(r)\cos n\theta\cos(\omega_n t+\alpha) \tag{4}$$

where ζ_A and ζ_B are the amplitudes of the stator particles excited by the voltages, α is the phase difference of exciting voltages, ω_n is the frequency of the nth-order vibration mode.

The displacement of the stator considering the superposition principle can be described as

$$\begin{aligned}\varpi = \varpi_A + \varpi_B &= \frac{1}{2}(\zeta_A - \zeta_B\sin\alpha)J_n(r)\sin(n\theta+\omega_n t)\\ &+\frac{1}{2}(\zeta_A+\zeta_B\sin\alpha)J_n(r)\sin(n\theta-\omega_n t)\\ &+\zeta_B J_n(r)\cos\alpha\cos n\theta\cos\omega_n t.\end{aligned} \tag{5}$$

It can be concluded that the vibration of the stator consists of the forward traveling wave $\sin(n\theta - \omega_n t)$, the backward traveling wave $\sin(n\theta + \omega_n t)$ and the standing wave $\cos n\theta \cos \omega_n t$.

If α is $\pi/2$ and the values of ζ_A, ζ_B, and ζ_0 are the same, the forward traveling wave described by (5) can be given as

$$\varpi(r, \theta, t) = \zeta_0 J_n(r) \sin(n\theta - \omega_n t). \tag{6}$$

If α is $-\pi/2$ and the values of ζ_A, ζ_B, and ζ_0 are the same, the backward traveling wave described by (5) can be given as

$$\varpi(r, \theta, t) = \zeta_0 J_n(r) \sin(n\theta + \omega_n t). \tag{7}$$

It can be concluded that the traveling wave generation condition of the stator is that the phase difference of the exciting signals is $\pi/2$. The spatial difference between the two excited standing waves should also be $\pi/2$ [18].

For the proposed motor, four groups of PZT components are nested into the stator to excite the traveling wave. Two nonadjacent PZT components are utilized to excite B_{0n} axial bending mode. The polarization and placements of the PZT components are shown in Fig. 1(c). A phase-A PZT component is composed of the PZT component A and C, and a phase-B PZT component is composed of the PZT component B and D. Four PZT ceramics of one component are parallel with each other. The polarization directions of the PZT ceramics are opposite to the adjacent ones. The sinusoidal alternating voltage is generated to the phase-A PZT component. A standing wave can be excited through the alternating expansion and contraction of the PZT components. Similarly, another standing wave can be excited through applying cosine alternating voltage to phase-B PZT component. The phase difference between the exciting voltages is $\pi/2$ which ensures the phase difference between the two standing waves is $\pi/2$.

The unfolded-drawings of the stator and the generation of the traveling wave are shown in Fig. 2.

1) When $t = 0$, the direction of the exciting voltage is the same as the polarization direction of the PZT component A. The PZT component A is in tension state; the position of the PZT component A is a peak. The exciting voltage is opposite to the polarization direction of the PZT component C. The PZT component C is in compression state and its position is a valley.
2) When $t = T/4$, the PZT component B is in tension state and its position is a peak. The traveling wave moves a quarter of a wavelength forward.
3) When $t = T/2$, the vibration displacements of the PZT component A and C are the largest. However, the PZT A is in compression state and the PZT C is in tension state. Thus, the position of the PZT component C is a peak and the position of the PZT component A is a valley.
4) When $t = 3T/4$, the vibration mode is contrary to $t = T/4$, the position of the PZT component D is a peak.
5) When $t = T$, the traveling wave moves a wavelength forward and the vibration mode of the stator returns to the initial state.

IV. Analysis and Simulation

First, modal analysis was conducted in this section to obtain the vibration modes and the resonant frequencies of the prototype. The adhesives between the PZT ceramics and the copper electrodes were ignored because they were too thin. The modeling parameters of the traveling wave USM were listed in Table I. The driving tips of the prototype were designed at the bottom of the stator. Thus, the B (0, 5) axial bending vibration mode was selected to achieve the elliptical trajectories at the driving tips.

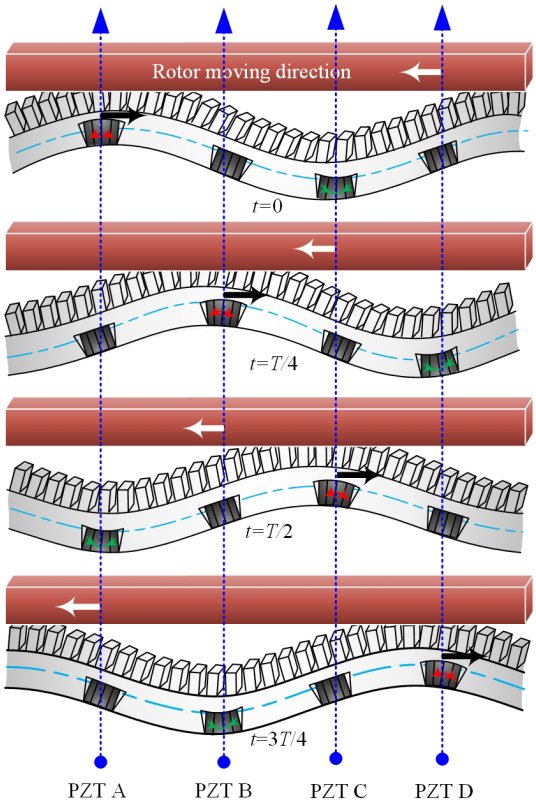

Fig. 2. Driving mechanism of the traveling wave USM.

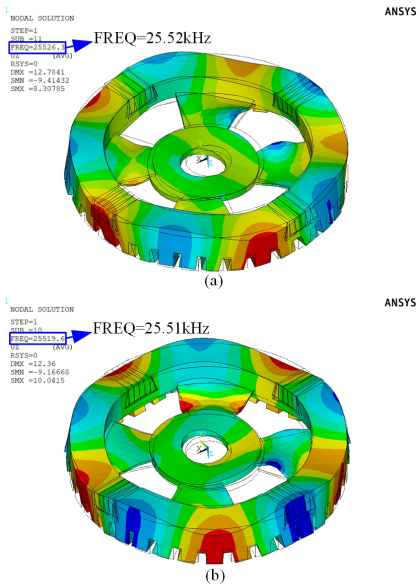

Fig. 3. Vibration modes of the proposed traveling wave USM. (a) Mode-A. (b) Mode-B.

TABLE I
STRUCTURE PARAMETERS OF TRAVELING WAVE USM

Symbols	Parameters	Values
D_1	External diameter of the stator	60mm
D_2	Internal diameter of the stator	45mm
D_3	Internal diameter of the driving tip	52mm
d_1	External diameter of the hub	24mm
d_2	Internal diameter of the hub	10mm
h_1	Height of the driving tip	3.5mm
h_2	Thickness of the ring-shape stator	6mm
h_3	Thickness of the hub	1.5mm
h_4	Thickness of the supporting rib	0.5mm
h_5	Height of the wedging block	4.2mm
a	Upper length of the wedging block	0.54mm
θ_1	Included angle of the supporting rib	45°
θ_2	Angle between adjacent supporting ribs	45°
θ_3	Included angle of wedging block	10°
n_1	Number of driving tips	35

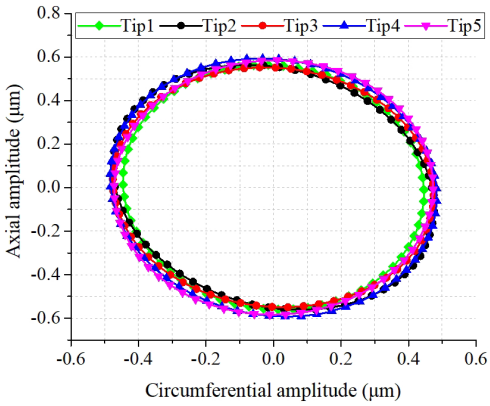

Fig. 4. Simulation elliptical trajectories of five adjacent driving tips.

As shown in Fig. 3, the B (0, 5) axial bending vibration modes were obtained by modal analysis. The resonant frequencies of two B (0, 5) axial bending vibration modes are 25.51 and 25.52 kHz, respectively. It can be found that there is a quarter wavelength spatial difference between these two modes. The temporal difference of $\pi/2$ between the two modes can be generated through the exciting voltages. Theoretically, the vibration modes obtained by the modal analysis satisfy the generation condition of traveling wave.

Second, based on the result of the modal analysis, two ac voltages with a phase difference of $\pi/2$, voltage of 141 V_{p-p} and frequency of 25.51 kHz were applied to the two groups of the PZT ceramics to accomplish the transient analysis. To investigate the movement behavior of the driving tips, the trajectories of the center nodes were simulated, which were on the outer rims of five adjacent driving tips. As shown in Fig. 4, their trajectories are ellipses, and the differences of these trajectories in circumferential and axial directions are small. This phenomenon proves that driving tips have

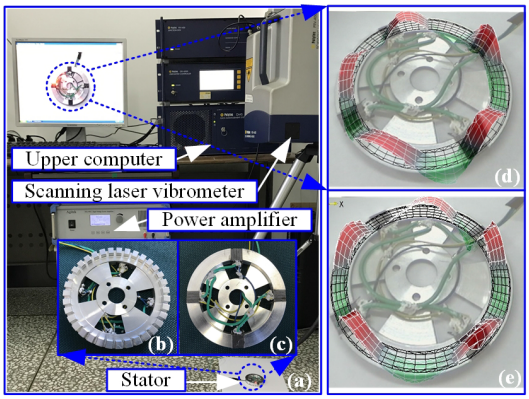

Fig. 5. Vibration scanning of the prototype. (a) Vibration scanning devices. (b) Bottom of the prototype. (c) Top of the prototype. (d) Vibration mode of phase-A. (e) Vibration mode of phase-B.

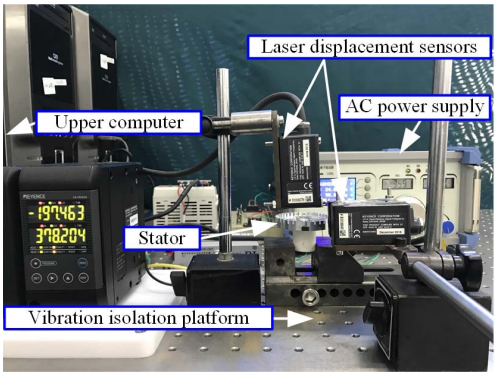

Fig. 6. Experiment setup for measuring the elliptical trajectories of the prototype.

uniform movements. The average axial and circumferential amplitudes are 1.14 and 0.94 μm.

V. EXPERIMENTAL VALIDATION

After the simulation analysis, the proposed traveling wave USM was manufactured according to the parameters in Table I. As shown in Fig. 5, the vibration modes and resonant frequencies of the prototype were tested by a scanning laser Doppler vibrometer (Model: PSV-400-M2, Polytec, Waldbronn, Germany). The two vibration modes were tested, and the phase-A PZT component or phase-B PZT component was connected to the high potential terminal of a power amplifier (Model: ATA-4051, AIGTEK, BEIJING, CHINA). The measuring results indicate that the resonant frequencies of B (0, 5) axial bending vibration modes are 25.35 and 24.95 kHz, which have differences of 0.16 and 0.57 kHz compared with the simulation results. These differences are mainly caused by manufacturing and assembling errors. The scanned vibration modes of the prototype in Fig. 5 are the same as the ones designed in Fig. 3. Thus, the prototype designed in the simulation environment has been proven preliminarily through the vibration test.

The moving trajectories and the operating principle of the proposed traveling wave USM were validated by the measuring system in Fig. 6. An ac power supply was used to generate exciting voltages with a phase difference of $\pi/2$.

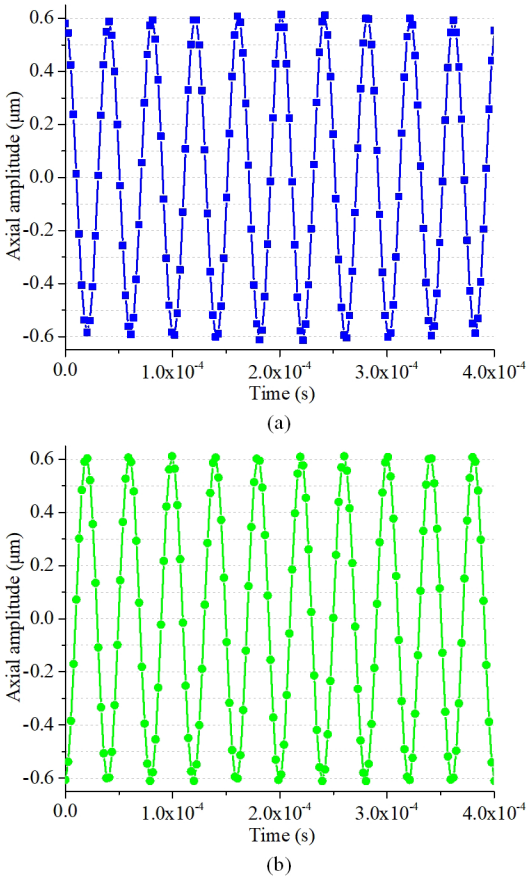

Fig. 7. Amplitudes of two standing waves. (a) Amplitudes of phase-A. (b) Amplitudes of phase-B.

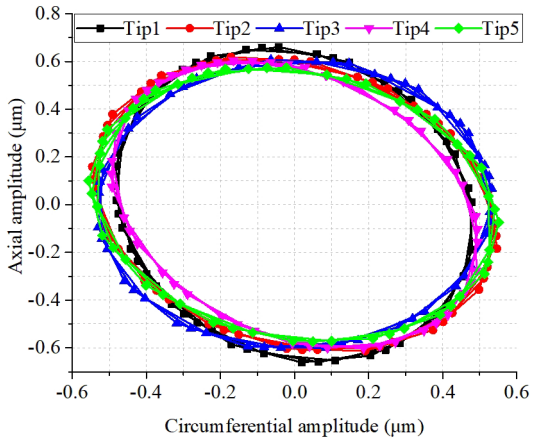

Fig. 8. Elliptical trajectories of five adjacent driving tips.

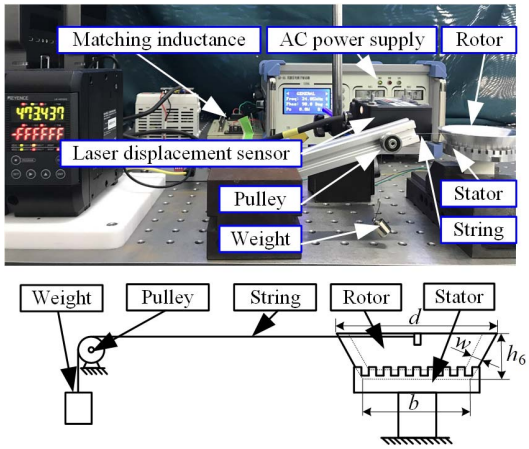

Fig. 9. Experiment setup for measuring the mechanical output performance of the prototype.

The output voltage of the ac power supply could be adjusted from 0 to 600 V_{p-p}. The exciting voltages were applied to phases A and B PZT components to excite the stator. Two laser displacement sensors (Model: LK-H020, KEYENCE, OSAKA, JAPAN) were used to measure the displacements on the driving tips in axial and circumferential directions.

One of the ideal traveling wave generation conditions is that the amplitudes of the two standing waves should be the same. The different amplitudes can cause traveling wave distortion. Thus, the amplitudes of two standing waves should be discussed first. During the standing wave exciting experiment, phase-A or phase-B PZT component was connected to the high potential terminal of the ac power supply and the stator was connected to the low potential terminal. The input voltage was set to 141 V_{p-p} and the exciting frequency was set from 23 to 27 kHz which was related to the measured resonant frequencies. When the exciting frequency was 24.86 kHz, as shown in Fig. 7, ten cycles of the amplitudes of one driving tip were recorded by the laser displacement sensor. The average amplitudes of phase-A and phase-B PZT components are 1.19 and 1.21 μm, which have differences of 0.05 and 0.07 μm compared with the simulation results. The differences are about 4.39% and 6.14% of the simulation amplitudes. The amplitudes of two standing waves are almost the same, which proves that the prototype satisfies one of the requirements for generating the traveling wave.

According to the operating principle of the prototype, the realization of the elliptical trajectory is one of the most important design objects of the traveling wave USM. The trajectories of five adjacent driving tips were measured by two laser displacement sensors. These five driving tips were the same as the driving tips in the simulation. The exciting voltage was 141 V_{p-p}, and the exciting frequency was 24.86 kHz. As shown in Fig. 8, the motion trajectories of these five nodes were compared in the same coordinate system. The motion trajectories of these five adjacent driving tips are ellipses. The average axial and circumferential amplitudes are 1.20 and 1.01 μm, which have differences of 0.06 and 0.07 μm compared with the simulation results. The differences are about 5.26% and 7.45% of the simulation amplitudes. Experimental results are similar to the simulation results and the deviations are small.

The mechanical output performances of the prototype were tested by the experimental setup shown in Fig. 9. First, an aluminum alloy conning rotor was fabricated to research the relationship between the exciting frequency and the output speed. The structural parameters of the conning rotor were as follows, the top diameter d was 70 mm, the bottom diameter b was 49 mm, the height h_6 was 15 mm, the thickness w was 3 mm.

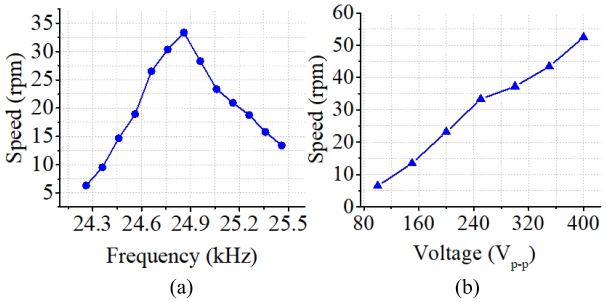

Fig. 10. Speed characteristics of the prototype. (a) Speed characteristics versus frequencies. (b) Speed characteristics versus voltages.

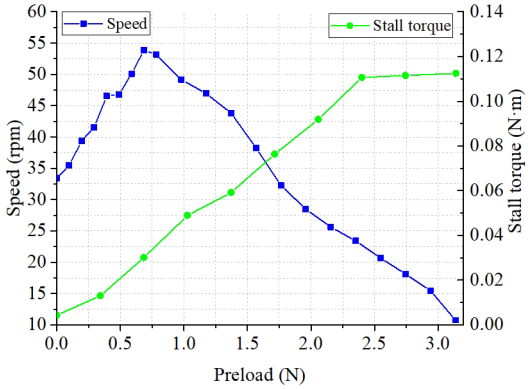

Fig. 11. Speed and stall torque characteristics versus preloads.

To find the proper working frequency, the exciting voltage was set to 250 V_{p-p}, and no preload was generated to the rotor. The exciting frequency was set from 24.26 to 25.46 kHz, which was related to the resonant frequency of the phase-A and phase-B PZT components. As shown in Fig. 10(a), the maximum speed of 33.36 r/min is achieved under the frequency of 24.86 kHz.

Second, the relationship between the exciting voltage and the output speed was researched. During the measuring process, no preload was applied. The preload force applied to the stator was completely dependent on the weight of the coning rotor. The voltage was set from 100 to 400 V_{p-p}. The exciting frequency was set to 24.86 kHz, which was the optimal frequency. As shown in Fig. 10(b), the speed increases as the exciting voltage increases. The maximum speed is 52.45 r/min, which is obtained when the exciting voltage is 400 V_{p-p}.

The energy generated by traveling wave USM is transmitted through the contact friction between the rotor and the stator [19], [20]. Friction is related to the weight of the rotor and the preload generated to the rotor. Thus, the preload also affects the speed of the rotor. The exciting voltage was set to 250 V_{p-p}, and the exciting frequency was set to 24.86 kHz. Different weights were added to the rotor to adjust the preload. As shown in Fig. 11, the speed increases as the preload increases from 0 to 0.69 N. The maximum speed is 53.86 r/min, which is measured when the preload is 0.69 N. However, the speed of the coning rotor decreases to 10.75 r/min as the preload increases to 3.14 N. Experimental results indicate that the relationship between the preload and

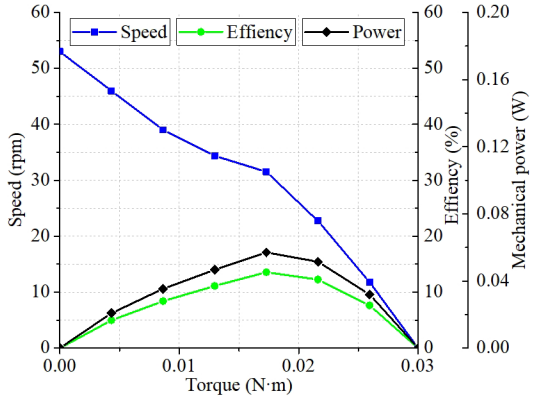

Fig. 12. Mechanical output characteristics.

the speed is not linear. The proper preload may improve the output characteristic of the traveling wave USM. As for the proposed traveling wave USM, the proper preload is 0.69 N if the speed is the most important index.

The performances of the output mechanical power and the efficiency of the proposed motor were also researched in this work. The exciting voltage was set to 250 V_{p-p}, and the exciting frequency was set to 24.86 kHz and the preload was set to 0.69 N, which is the optimal preload. The efficiency of the prototype in this experiment was calculated by (8). As shown in Fig. 12, the peak efficiency is 13.57% when the peak power is 0.06 W

$$\eta = \frac{J\omega^2}{2t_1 P_0} \tag{8}$$

where J is the inertia moment of the rotor, ω is the speed of the rotor, t_1 is the time. P_0 is the input power measured by digital power meter (Model: WT210, YOKOGAWA, TOKYO, JAPAN).

But in some applications of traveling wave USM, the output torque needs to be considered first. In this situation, the higher preload can bring a better output characteristic. The stall torque of the prototype was measured. The rotor and the weight were connected through a string. The exciting voltage was set to 250 V_{p-p}, and the exciting frequency was set to 24.86 kHz. Different weights were added to the rotor. As shown in Fig. 11, the relationship between the stall torque and the preload of the motor was researched. The result indicates that the stall torque increases as the preload increases. The maximum stall torque is 0.11 N · m when the preload is 3.14 N.

The comparison between the previous motor and this design was presented in Table II. Compared with the previous motor, the weight decreases from 3.17 to 0.03 kg; the volume of the PZT ceramics decreases from 82 978 to 720 mm^3. Besides, the power density is enhanced from 1.26 to 2.0 W/kg, the torque density is improved from 2.51 to 3.67 N · m/kg, the efficiency is enhanced from 9% to 13.57%, the no-load speed is increased from 15 to 33.36 r/min. It should be noted that the resonant frequencies of the two modes of the prototype still have a discrepancy of 400 Hz, which means that the mechanical output performances of the proposed motor can be improved further by tuning them closer to each other.

TABLE II
COMPARISONS WITH THE PREVIOUS MOTOR

Parameters	This work	Previous work [17]
Diameter of the stator (mm)	60	157
Weight (kg)	0.03	3.17
Group number of the PZTs	4	64
Volume of the PZT ceramics (mm^3)	720	82978
Total number of the PZTs	16	128
No-load speed (rpm)	33.36	15
Torque density (N·m/kg)	3.67	2.51
Efficiency (%)	13.57	9
Power density (W/kg)	2.0	1.26

VI. CONCLUSION

A rotary USM with four groups of nested PZT ceramics was designed, manufactured and tested. Two axial bending standing waves with the spatial phase shift of a quarter wavelength were generated to form a traveling wave. The B (0, 5) axial bending vibration modes of the stator and elliptical trajectories of the driving tips were simulated by the FEM. The vibration shapes of the ring-shaped stator were tested, which were consistent with the FEM calculated results. When the input voltage was set to 141 V_{p-p}, the elliptical trajectories of five adjacent driving tips were tested and the average amplitudes of these trajectories in axial and circumferential direction were 1.20 and 1.01 μm, which had errors of 5.26% and 7.45% relative to the simulation results. The mechanical output performances of the prototype were tested. The experiment results validated that the new prototype with nested PZT ceramics achieved a notable improvement in some of the mechanical output characteristics with the significant reduction in the volume and weight, such as the no-load speed of 33.36 r/min, the efficiency of 13.57%, the torque density of 3.67 N · m/kg and the power density of 2.0 W/kg. This study provides a new method to reduce the volume of the traveling wave USM with ring-shaped stator and improve its output speed, torque density, efficiency and power density.

REFERENCES

[1] M. Kuhne, R. G. Rochin, R. S. Cos, G. J. R. Astorga, and A. Peer, "Modeling and two-input sliding mode control of rotary traveling wave ultrasonic motors," *IEEE Trans. Ind. Electron.*, vol. 65, no. 9, pp. 7149–7159, Sep. 2018.

[2] S. Ghenna, F. Giraud, C. Giraud-Audine, and M. Amberg, "Vector control of piezoelectric transducers and ultrasonic actuators," *IEEE Trans. Ind. Electron.*, vol. 65, no. 6, pp. 4880–4888, Jun. 2018.

[3] L. Wang, Y. Wang, X. Lu, and C. Zhao, "Note: A disk-shaft shaped high-speed rotary ultrasonic motor," *Rev. Sci. Instrum.*, vol. 89, no. 12, Dec. 2018, Art. no. 126106.

[4] P. Hareesh and D. L. Devoe, "Miniature bulk PZT traveling wave ultrasonic motors for low-speed high-torque rotary actuation," *J. Microelectromech. Syst.*, vol. 27, no. 3, pp. 547–554, Jun. 2018.

[5] Y. Luan, B. Lin, X. Ma, and X. Zhu, "Innovative contactless energy transfer accessory for rotary ultrasonic machining and its circuit compensation based on coil turns," *IEEE Trans. Ind. Electron.*, vol. 64, no. 10, pp. 7810–7818, Oct. 2017.

[6] T. Mashimo, "Scaling of piezoelectric ultrasonic motors at submillimeter range," *IEEE/ASME Trans. Mechatronics*, vol. 22, no. 3, pp. 1238–1246, Jun. 2017.

[7] J. Wu, Y. Mizuno, and K. Nakamura, "Polymer-based ultrasonic motors utilizing high-order vibration modes," *IEEE/ASME Trans. Mechatronics*, vol. 23, no. 2, pp. 788–799, Apr. 2018.

[8] K. Nakamura, M. Kurosawa, and S. Ueha, "Characteristics of a hybrid transducer-type ultrasonic motor," *IEEE Trans. Ultrason., Ferroelectr., Freq. Control*, vol. 38, no. 3, pp. 188–193, May 1991.

[9] K. Takemura and T. Maeno, "Design and control of an ultrasonic motor capable of generating multi-DOF motion," *IEEE/ASME Trans. Mechatronics*, vol. 6, no. 4, pp. 499–506, Dec. 2001.

[10] C.-H. Cheng and S.-K. Hung, "A piezoelectric two-degree-of-freedom nanostepping motor with parallel design," *IEEE/ASME Trans. Mechatronics*, vol. 21, no. 4, pp. 2197–2199, Aug. 2016.

[11] Z. Zhu, S. To, K. F. Ehmann, and X. Zhou, "Design, analysis, and realization of a novel piezoelectrically actuated rotary spatial vibration system for micro-/nanomachining," *IEEE/ASME Trans. Mechatronics*, vol. 22, no. 3, pp. 1227–1237, Jun. 2017.

[12] Y. Ting, L. C. Chen, and C. C. Li, "Traveling-wave piezoelectric linear motor part I: The stator design," *IEEE Trans. Ultrason., Ferroelectr., Freq. Control*, vol. 54, no. 4, pp. 847–853, Apr. 2007.

[13] J.-S. Park, S.-T. Kim, J.-W. Kim, J.-K. Lee, and K. S. Hong, "Ultrasonic linear motor using L1-B4 mode and its analysis," *Jpn. J. Appl. Phys.*, vol. 44, no. 1A, pp. 412–416, Jul. 2005.

[14] L. Petit and P. Gonnard, "A multilayer TWILA ultrasonic motor," *Sens. Actuators A, Phys.*, vol. 149, no. 1, pp. 113–119, Jan. 2009.

[15] W. Chen, Y. X. Liu, and X. Yang, "Ring-type traveling wave ultrasonic motor using a radial bending mode," *IEEE Trans. Ultrason., Ferroelectr., Freq. Control*, vol. 61, no. 1, pp. 197–202, Jan. 2014.

[16] Y.-X. Liu, J.-K. Liu, W.-S. Chen, and X.-H. Yang, "A rotary ultrasonic motor using radial bending mode of ring with nested PZT excitation," *J. Zhejiang Univ. Sci. A*, vol. 13, no. 3, pp. 189–196, Mar. 2012.

[17] W. Chen, S. Shi, Y. Liu, and P. Li, "A new traveling wave ultrasonic motor using thick ring stator with nested PZT excitation," *IEEE Trans. Ultrason., Ferroelectr., Freq. Control*, vol. 57, no. 5, pp. 1160–1168, May 2010.

[18] C. Zhao, *Ultrasonic Motors: Technologies and Applications*, 1st ed. Springer, Jan. 2011, pp. 160–167.

[19] H. Huang *et al.*, "Note: A novel rotary actuator driven by only one piezoelectric actuator," *Rev. Sci. Instrum.*, vol. 84, no. 9, Sep. 2013, Art. no. 096105.

[20] A. Iula and M. Pappalardo, "A high-power traveling wave ultrasonic motor," *IEEE Trans. Ultrason., Ferroelectr., Freq. Control*, vol. 53, no. 7, pp. 1344–1351, Jul. 2006.

Xuefeng Ma was born in Heilongjiang, China, in 1993. He received the B.E. degree in mechatronic engineering from the Harbin University of Commerce, Harbin, China, in 2016, and the M.E. degree from the School of Mechatronics Engineering, Harbin University of Science and Technology, Harbin, in 2019. He is currently pursuing the Ph.D. degree in mechatronic engineering with the Harbin Institute of Technology, Harbin.

His research interests include the precision piezoelectric actuators and ultrasonic motors.

Junkao Liu was born in Hebei, China, in 1973. He received the B.E. degree in mechanical engineering and the Ph.D. degree in mechatronics engineering from the School of Mechatronics Engineering, Harbin Institute of Technology, Harbin, China, in 1995 and 2001, respectively.

Since 2011, he has been a Professor with the School of Mechatronics Engineering, Harbin Institute of Technology. His research interests include ultrasonic driving, biomimetic robots, and simulations of parallel mechanisms with multi-degree of freedom.

Jie Deng was born in Shaanxi, China, in 1992. He received the B.E. degree in mechanical engineering from the School of Mechanical Engineering, Northwestern Polytechnical University, Xi'an, China, in 2014, and the M.E. degree in mechatronics engineering from the School of Mechatronics Engineering, Harbin Institute of Technology, Harbin, China, in 2016, where he is currently pursuing the Ph.D. degree in mechatronics engineering.

His research interests include ultrasonic motor and precision piezoelectric actuating platform with multi-DOF.

Qiang Liu was born in Chifeng, Inner Mongolia, China in 1981.He received the B.E. degree in mechanical engineering from the Harbin Institute of Technology, Harbin, China, in 2005, and the Ph.D. degree in optical engineering from the University of Chinese Academy of Sciences, Beijing, China, in 2013.

He is currently an Associate Researcher with the Changchun Institute of Optics, Fine Mechanics and Physics, Chinese Academy of Sciences, Beijing. His research interests include optical remote sensor design, precision drive, and support structure design.

Yingxiang Liu (Senior Member, IEEE) was born in Hebei, China, in 1982. He received the B.E. degree in mechanical engineering, and the M.E. and Ph.D. degrees in mechatronics engineering from the School of Mechatronics Engineering, Harbin Institute of Technology, Harbin, China, in 2005, 2007, and 2011, respectively.

He joined the School of Mechatronics Engineering, Harbin Institute of Technology in 2011, where he has been a Professor since December 2013, and also a Member of the State Key Laboratory of Robotics and System. He was a Visiting Scholar with the Mechanical Engineering Department, University of California at Berkeley, Berkeley, CA, USA, from August 2013 to August 2014. He is currently the Vice Director with the Department of Mechatronic Control and Automation, Harbin Institute of Technology. His research interests include piezoelectric (PZT) actuating, ultrasonic motors, PZT actuators, precision actuating, PZT microjets, bionic robots, fish robots, and soft robots.

Dr. Liu served as an Associate Editor for the IEEE TRANSACTIONS ON INDUSTRIAL ELECTRONICS, IEEE ACCESS, and a Guest Editor of *Applied Sciences*.